Electrochemical Preparation of Molybdenum Trioxide Thin Films: Effect of Sintering on Electrochromic and Electroinsertion Properties

Todd M. McEvoy and Keith J. Stevenson*

Department of Chemistry and Biochemistry, Center for Nano- and Molecular Science and Technology, Texas Materials Institute, University of Texas at Austin, Austin, Texas 78712

Joseph T. Hupp

Department of Chemistry, Center for Nanofabrication and Molecular Self-Assembly, Northwestern University, Evanston, Illinois 60208

Xiaojun Dang

Ondeo Nalco Company, Naperville, Illinois 60563

Received December 17, 2002. In Final Form: February 24, 2003

Molybdenum trioxide (MoO_3) thin films prepared by cathodic electrodeposition on indium−tin-oxide coated glass substrates from aqueous peroxo-polymolybdate solutions have been studied as a function of sintering temperature (25−450 °C). Cyclic voltammetry, chronopotentiometry, chronoamperometry, and spectroelectrochemical measurements performed with MoO_3 thin films in 1 M $LiClO_4$/propylene carbonate demonstrate that the electrochemical behavior (Li^+ insertion/extraction and coloration) is strongly dependent upon thermally induced changes in micro-/nanocrystallinity, which directly influence measured Li^+ diffusion properties as well as electroinsertion and electrochromic reversibilities. Structural analysis using X-ray photoelectron spectroscopy, X-ray diffraction, and atomic force microscopy indicate that films heat treated at 100 °C or less exist as amorphous oxide-hydrates of molybdenum; whereas films heated to 250 °C exist as disordered, mixed-phase materials comprising monoclinic β-MoO_3 and orthorhombic α-MoO_3. Crystallization to the more thermodynamically stable orthorhombic α-MoO_3 occurs at 350 °C and above. The mixed-phase material exhibits inhomogeneous electrochemical activity, evidenced by the existence of complicated voltammetric and chronoamperometric responses. The effects of sintering temperature on ion insertion and electrocoloration properties are discussed.

1. Introduction

Redox-active transition metal oxides (i.e., V_2O_5, MoO_3, WO_3) have shown considerable promise for application in the areas of electrochromics[1] and batteries.[2] The electrochromic effect observed in these materials has led to their use in the development of displays[3,4] and smart windows.[5,6] Smart window fabrication has seen the greater extent of advancement between the two with the major thrust arising from a need for more efficient control over heating and cooling conditions in office buildings.[7] Development of new and improved electrochromic devices centers on increasing coloration efficiency and cycle life in addition to decreasing coloration response time. More recently, attempts at enhancing these properties have focused on fabrication of materials with nanoscale dimensions[3,4] in hopes that structural modification on such small size scales will ultimately lead to improvement in switching times and amplification of the electrochromic response through reduction of diffusion lengths and increased surface area. Added interest in these materials for use in energy storage systems is fueled, in part, by the desire to maximize energy stored per unit mass, in addition to improving structural stability over numerous charge/discharge cycles. For cathode materials used in rechargeable batteries (i.e., metal chalcogenides or oxides), it has been found that the component particle size and chemical structure greatly determine the resulting energy density and power performance.[8−10] Kim and co-workers[10] have shown that composite electrodes utilizing nanocrystals of $LiMnO_4$ (50−100 nm in length) exhibited a greater insertion capacity than when larger particles of $LiMnO_4$ (0.5−2 μm) were used. Synthesis of small metal oxide particles using conventional solid state reaction methodologies is often difficult because these methods generally necessitate extended heat treatments at high temperatures that typically lead to the formation of large particle aggregates.

* To whom correspondence may be addressed: fax, 512-471-8696; e-mail address, stevenson@mail.cm.utexas.edu.

(1) Granqvist, C. G. *Handbook of Inorganic Electrochromic Materials*, 1st ed.; Elsevier: Amsterdam, 1995.
(2) Winter, M.; Besenhard, J. O.; Spahr, M. E.; Novak, P. *Adv. Mater.* **1998**, *10*, 725.
(3) Bach, U.; Corr, D.; Lupo, D.; Pichot, F.; Ryan, M. *Adv. Mater.* **2002**, *14*, 845.
(4) Liu, J.; Coleman, J. P. *Mater. Sci. Eng., A* **2000**, *A286*, 144.
(5) Granqvist, C. G.; Azens, A.; Hjelm, A.; Kullman, L.; Niklasson, G. A.; Ronnow, D.; Stromme Mattsson, M.; Veszelei, M.; Vaivars, G. *Sol. Energy* **1998**, *63*, 199.
(6) Sella, C.; Maaza, M.; Nemraoui, O.; Lafait, J.; Renard, N.; Sampeur, Y. *Surf. Coat. Technol.* **1998**, *98*, 1477.
(7) Somani, P. R.; Radhakrishnan, S. *Mater. Chem. Phys.* **2002**, *77*, 117.
(8) Lu, C.-H.; Lin, S.-W. *J. Power Sources* **2001**, *97−98*, 458.
(9) Hwang, K.-T.; Um, W.-S.; Lee, H.-S.; Song, J.-K.; Chung, K.-W. *J. Power Sources* **1998**, *74*, 169.
(10) Choy, J.-H.; Kim, D.-H.; Kwon, C.-W.; Hwang, S.-J.; Kim, Y.-I. *J. Powers Sources* **1999**, *77*, 1.

10.1021/la027020u CCC: $25.00
Published on Web 03/27/2003

While several vacuum-based techniques have been reported (i.e., pulsed laser ablation,[11] thermal evaporation,[12,13] and sputtering[14]) for fabrication of MoO_3 thin films, we are particularly interested in using electrochemical deposition[15,16] and soft solution processing techniques[17,18] in combination with templating methodologies[19−21] to control and assemble nanostructured cathode materials with interesting ionic and electronic transport characteristics to impart improved ion-storage and electrochromic properties. This low-cost, simple methodology offers several attractive advantages over other more high-energy-consuming, capital-intensive synthetic techniques such as sputtering and thermal evaporation. Some specific advantages include (1) rigid control of film thickness, uniformity, and deposition rate, (2) careful regulation over reaction parameters such as solution concentration and composition, and (3) facile adaptation to conformal deposition on substrates of complicated shape and geometry. Recently we have described the electrochemical synthesis of MoO_3 thin films via cathodic electrodeposition from an aqueous peroxo-polymolybdate solution.[22] Deposition at specific applied potentials provided us with a means for preparing thin films of molybdenum oxide with controlled stoichiometry, water content, and valency. However, we have observed that postdeposition heat treatment of these films at relatively low temperatures (≤450 °C) markedly influences the overall electroinsertion properties (insertion kinetics and charge storage capacity). While others[23−25] have briefly discussed the influence of sintering temperature on structural features and electroinsertion properties of electrodeposited MoO_3 thin films, to our knowledge no detailed investigations concerning the effect of film microstructure, metal oxidation state, and water content on the electrochromic and ion storage behavior have been reported.

Herein, we discuss the influence of postdeposition sintering in air on the microstructure and electroinsertion/electrocoloration properties of electrodeposited MoO_3 thin films. MoO_3 thin films are characterized by a number of techniques, allowing for correlation of morphological characteristics with optical and electrochemical properties.

2. Experimental Section

MoO_3 Thin Film Preparation. We have recently reported in detail the electrodeposition of MoO_3 thin films from acidic peroxo-polymolybdate solutions.[22] However, we briefly summarize our preparation methodology for films used in this study. Transparent, conductive indium−tin-oxide (ITO) coated glass substrates (Delta Technologies, Ltd., 15 Ω/□) were cleaned by immersion for 10 min in a heated (80 °C) aqueous solution of ethanolamine (Aldrich, 30 vol %). The substrates were then rinsed several times with ultrapure (Barnestead, Nanopure II, 18 MΩ·cm) water, followed by sonication in ultrapure water for 1 h, and finally dried under a stream of nitrogen. Following the route described by Guerfi et al.,[15,16] aqueous molybdenum deposition solutions were prepared by dissolving 1 g of molybdenum foil (Alfa Aesar, 99.95%) in 6 mL of 30% (v/v) aqueous hydrogen peroxide solution (Mallinckrodt). When the metal was completely dissolved and the exothermic reaction had ended, platinum black, prepared by a previously published procedure,[26] was added to reduce the excess peroxide. The solution was diluted to 100 mL volume with ultrapure water resulting in an approximate molybdenum content of 0.1 M. The ITO-coated glass substrates, acting as the working electrode, were then placed in the aqueous molybdenum oxide deposition solution along with a Ag/AgCl reference electrode (BAS, 3 M NaCl), and a platinum wire (Aldrich) serving as the counter electrode. Blue-colored thin films were obtained by applying a fixed potential of −0.02 V vs Ag/AgCl for a predetermined length of time. As previously reported,[22] electrochemical quartz crystal microbalance studies indicate that deposition at this potential is consistent with the formation of a mixed-valent substoichiometric molybdenum oxide, comprising Mo^{VI}/Mo^{V}, with a chemical composition of $\sim MoO_{2.7}\cdot 2H_2O$. As shown in Figure 1, the film thicknesses, *d*, for freshly as-deposited and heat-treated films were measured with atomic force microscopy (AFM). The freshly as-deposited film thickness could

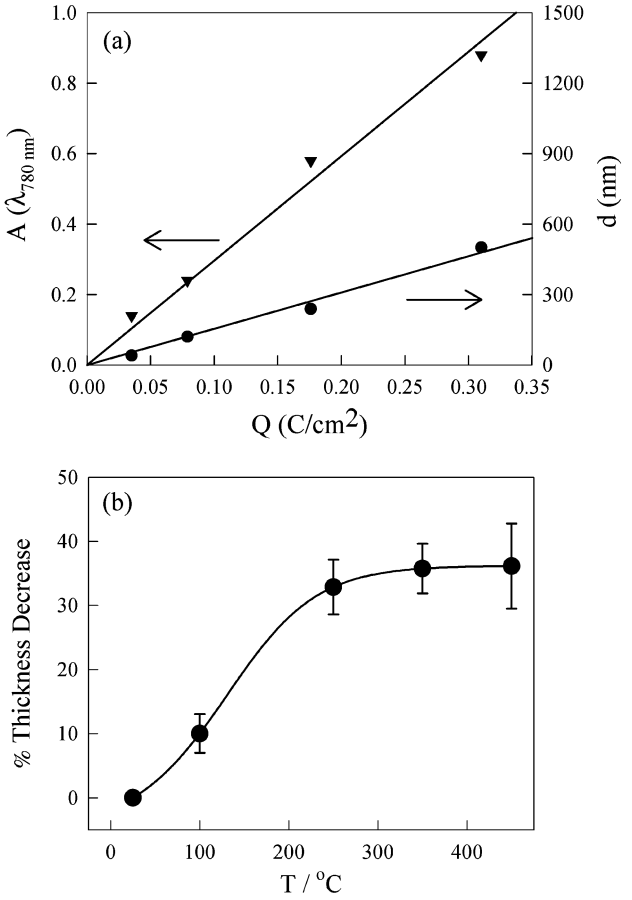

Figure 1. (a) Plot of deposition charge density for the electrodeposition of a MoO_3 thin film on ITO versus AFM-measured film thickness, *d*, and UV−vis-measured absorbance (λ = 780 nm). (b) Plot of percent decrease in film thickness versus sintering temperature. The line in (b) is drawn for visual reference.

(11) Iriyama, Y.; Abe, T.; Inaba, M.; Ogumi, Z. *Solid State Ionics* **2000**, *135*, 95.
(12) Yao, J. N.; Yang, Y. A.; Loo, B. H. *J. Phys. Chem. B* **1998**, *102*, 1856.
(13) Yang, Y. A.; Cao, Y. W.; Loo, B. H.; Yao, J. N. *J. Phys. Chem. B* **1998**, *102*, 9392.
(14) Ferriera, F. F.; Souza Cruz, T. G.; Fantini, M. C. A.; Tabacniks, M. H.; de Castro, S. C.; Morais, J.; de Siervo, A.; Landers, R.; Gorenstein, A. *Solid State Ionics* **2000**, *136−137*, 357.
(15) Guerfi, A.; Dao, L. H. *J. Electrochem. Soc.* **1989**, *136*, 2435.
(16) Guerfi, A.; Paynter, R. W.; Dao, L. H. *J. Electrochem. Soc.* **1995**, *142*, 3457.
(17) Rouxel, J.; Tournoux, M.; Brec, J. *Soft Chemistry Routes to New Materials*; Trans Tech Publications: Switzerland, 1993.
(18) Yoshimura, M.; Suchanek, W.; Han, K.-S. *J. Mater. Chem.* **1999**, *9*, 77.
(19) Muhr, H.-J.; Krumeich, F.; Schonholzer, U. P.; Bieri, F.; Niederberger, M.; Gauckler, L. J.; Nesper, R. *Adv. Mater.* **2000**, *12*, 231.
(20) Liu, P.; Zhang, J.-G.; Tracy, C. E.; Turner, J. A. *Electrochem. Solid-State Lett.* **2000**, *3*, 163.
(21) Stevenson, K. J.; Hurtt, G. J.; Hupp, J. T. *Electrochem. Solid-State Lett.* **1999**, *2*, 175.
(22) McEvoy, T. M.; Stevenson, K. J. *Anal. Chim. Acta*, in press.
(23) Belanger, D.; Laperriere, G. *Chem. Mater.* **1990**, *2*, 484.
(24) Laperriere, G.; Lavoie, M.-A.; Belanger, D. J. *Electrochem. Soc.* **1996**, *143*, 3109.
(25) Tsumura, T.; Inagaki, M. *Solid State Ionics* **1997**, *104*, 183.
(26) Bates, R. G. *Determination of pH: Theory and Practice*; John Wiley & Sons: New York, 1973; p 291.

be linearly correlated with both the charge passed during electrodeposition and the film absorbance, Figure 1a. This suggests that films are homogeneous with regard to film density and optical density (index of refraction). In the present study, all freshly deposited films were maintained at a constant thickness between 100 and 200 nm by ceasing deposition when the observed charge density reached ∼0.10 C/cm^2. Following deposition, the films were rinsed copiously with ultrapure water and then placed in a desiccator for 12 h to remove excess water prior to sintering. Postdeposition heat treatment without this step resulted in films with numerous stress-induced cracks present over the entire surface as water was removed from the film. The electrodeposited films were sintered in air using a Cress (model C401H/942) programmable electric furnace. The temperature was ramped from room temperature (∼25 °C) to a final temperature of 100, 250, 350, or 450 °C at a rate of 100 °C/h, whereupon the temperature was held for 3 h. After 3 h, the films were immediately removed from the furnace, allowed to cool, and stored in a desiccator. As shown in Figure 1b, heat treatment in air at temperatures ≥250 °C leads to film dehydration and densification resulting in ∼35% decrease in film thickness. Others[27] have reported a similar decrease in film thickness (∼28%) for thermally evaporated MoO_3 thin films heated to 180 °C. A 24% increase in (root mean square) surface roughness was also observed by AFM. A two-step dehydration process has been previously reported for bulk molybdenum oxide samples prepared by acidification of Na_2MoO_4[28−30] and for thin films prepared from peroxo-polymolybdate solution.[16,31] Loss of interlamellar water occurred by 100 °C producing a material consisting of sheets of disordered, corner sharing $MoO_5(H_2O)$ octahedra. A second dehydration step at ∼250 °C resulted from loss of closely coordinated water causing a topotactic shift along the *a*-axis to form a bilayer structure comprised of sheets MoO_6 octahedra that share bonds along octahedral edges. This two-step process is observed in Figure 1b, where a reduction in film thickness of 10% occurs when films are heated to 100 °C and a 33% decrease is observed when films are heated to 250 °C. Heat treatments above 450 °C were not attempted due to deformation/melting of the aluminosilicate/ ITO substrates above this temperature.

Structural Characterization. Atomic force microscopy was performed using a Digital Instruments Multimode Nanoscope IIIa or Digital Instruments Bioscope Nanoscope IV. All measurements were obtained in tapping mode with single etched silicon (TESP) Nanoprobe SPM tips (Digital Instruments, cantilever length 125 μm and resonance frequency ∼350 kHz). X-ray photoelectron spectra were acquired using a PHI 5700 ESCA system equipped with two X-ray sources. Incident X-rays for sample analysis were acquired using the Al Kα monochromatic (1486.6 eV) source. X-ray diffraction analysis was performed using a Rigaku Geigerflex X-ray diffractometer that employed a Cu $K\alpha_1$ line source. MoO_3/ITO samples were mounted on a fixed sample holder, and scattering intensity data were obtained in a $\theta/2\theta$ geometry with a rotating detector. The data were acquired between 5° and 40°. Data acquisition was performed every 0.2° with an integration time of 4 s.

Electrochemical Characterization. $LiClO_4$ (Aldrich) and anhydrous propylene carbonate (PC, Aldrich, 99.7%) were reagent grade and used as received. A conventional one-compartment, three-electrode Teflon cell, fitted with a Viton O-ring to provide a constant electrochemical area, was used for all electrochemical measurements unless otherwise noted. Pt wire (Aldrich) and Ag/AgCl (CH Instruments, 3 M KCl) electrodes were employed as the counter and reference electrodes, respectively, while the MoO_3 thin film served as the working electrode. The cell temperature was 25 ± 2 °C. Cyclic voltammetry and chronoamperometry were performed using a CH Instruments potentiostat (model CHI700A) interfaced to a personal computer. Cyclic voltammetry experiments were performed in a potential range from +0.4 to −0.8 V to avoid irreversible reduction of MoO_3 as well as to prevent solvent reduction/degradation. Chronoamperometry experiments were conducted using a 20 s potential step from +0.4 V, an initial potential where negligible current flows, to −0.8 V, a final value well beyond the thermodynamic reduction potential for MoO_3. Galvanostatic discharge/charge experiments were conducted using a CH Instruments (model 440) galvanostat/potentiostat interfaced to a personal computer. A current density of 10 μA/cm^2 was used for both discharging and charging MoO_3 thin films in 1 M $LiClO_4$/PC. Spectroelectrochemical characterization was carried out using a StellarNet EPP2000 fiber optic CCD UV−vis spectrometer coupled to a CH Instruments potentiostat (CHI700A). A standard spectroelectrochemical cell, consisting of a quartz cuvette and the three-electrode setup as described earlier, was used for all measurements. Optical absorption spectra were recorded every 2 s as the potential was scanned at 10 mV/s between +0.4 and −0.8 V vs Ag/AgCl. Optical microscopy images were acquired with a Roper Scientific CoolSNAP HQ CCD camera (0.100 s exposure time, cooled to −35 °C), mounted on a Nikon TE300 inverted optical microscope with a Nikon 60× 0.70 NA ELWD objective.

3. Results and Discussion

Structural Characterization. Figure 2 shows representative AFM images of films sintered from 100 to 450 °C. Examination of the AFM images shows that heat treatment at elevated temperatures produces changes in surface morphology. The AFM images indicate that the surfaces of films sintered at 100 °C consist of smooth, spherical-shaped grains ranging from ∼40 to 100 nm in diameter. However, films sintered at 250 °C appear to be composed of at least two components, one being randomly oriented partially crystalline domains formed from chains of aggregated MoO_3 particles and another which appears to be amorphous, or possibly nanocrystalline, in nature. Depending upon sintering conditions, the partially crystalline domains range in size from a few micrometers up to 10−15 μm in length. A higher resolution 1 × 1 μm^2 AFM image illustrating the formation of this layered phase is shown in Figure 3. Chains of small MoO_3 particles begin to coalesce at 250 °C (Figure 3a) to form larger, more crystalline, domains surrounded by regions of disordered MoO_3. As the sintering temperature is increased, larger crystalline domains emerge, and by 450 °C (Figure 3b) it appears that the entire surface is composed of randomly oriented, crystalline domains of layered MoO_3.

To examine the effect of sintering on Mo oxidation state, X-ray photoelectron spectroscopy (XPS) spectra were obtained for a film deposited on a Au substrate both before and after sintering at 250 °C for 3 h. The XPS spectra for the Mo $3d_{3/2}$, Mo $3d_{5/2}$, and O 1s core electronic transitions are shown in Figure 4. The XPS spectrum obtained from a blue-colored, as-deposited film, shown in Figure 4a, exhibits the characteristic $3d_{3/2}$ and $3d_{5/2}$ doublet of peaks at 235.9 and 232.8 eV, as is expected for a film comprised of Mo^{VI}.[32] However, the area ratio between the two peaks ($3d_{5/2}$:$3d_{3/2}$) was 5:4, which was not equal to the expected ratio of 3:2, as would be derived from the ratio of the peak degeneracies.[33] Since the peaks are wider than those of pure $Mo^{VI}O_3$, this implies that the film is composed of Mo^{VI} and a molybdenum species of lower oxidation state—presumably Mo^{V}. Upon sintering in air at 250 °C, a slight

(27) Al-Kuhaili, M. F.; Durrani, S. M. A.; Khawaja, E. E. *Thin Solid Films* **2002**, *408*, 188.
(28) Gunter, J. R. *J. Solid State Chem.* **1972**, *5*, 354.
(29) Boudjada, N.; Rodriguez-Carvajal, J.; Anne, M.; Figlarz, M. *J. Solid State Chem.* **1993**, *105*, 211.
(30) Kuzmin, A.; Purans, J. *J. Phys.: Condens. Matter* **2000**, *12*, 1959.
(31) Hinokuma, K.; Ogasawara, K.; Kishimoto, A.; Takano, S.; Kudo, T. *Solid State Ionics* **1992**, *53−56*, 507.
(32) National Institute of Standards and Technology X-ray Photoelectron Database, Web Version 3.2, 2000.
(33) For a stoichiometrically pure molybdenum oxide, all molybdenum would be in the +VI oxidation state. If this were the case, then the ratio of the peak degeneracies ($3d_{5/2}$:$3d_{3/2}$) would be 3:2. Since the observed ratio is somewhat less, we conclude that there is some Mo^{V} in the sample in addition to Mo^{VI}. See: *Practical Surface Analysis by Auger and X-ray Photoelectron Spectroscopy*, 2nd ed.; Briggs, D., Seah, M. P., Eds.; Wiley: New York, 1990; Vol. 1, p 113.

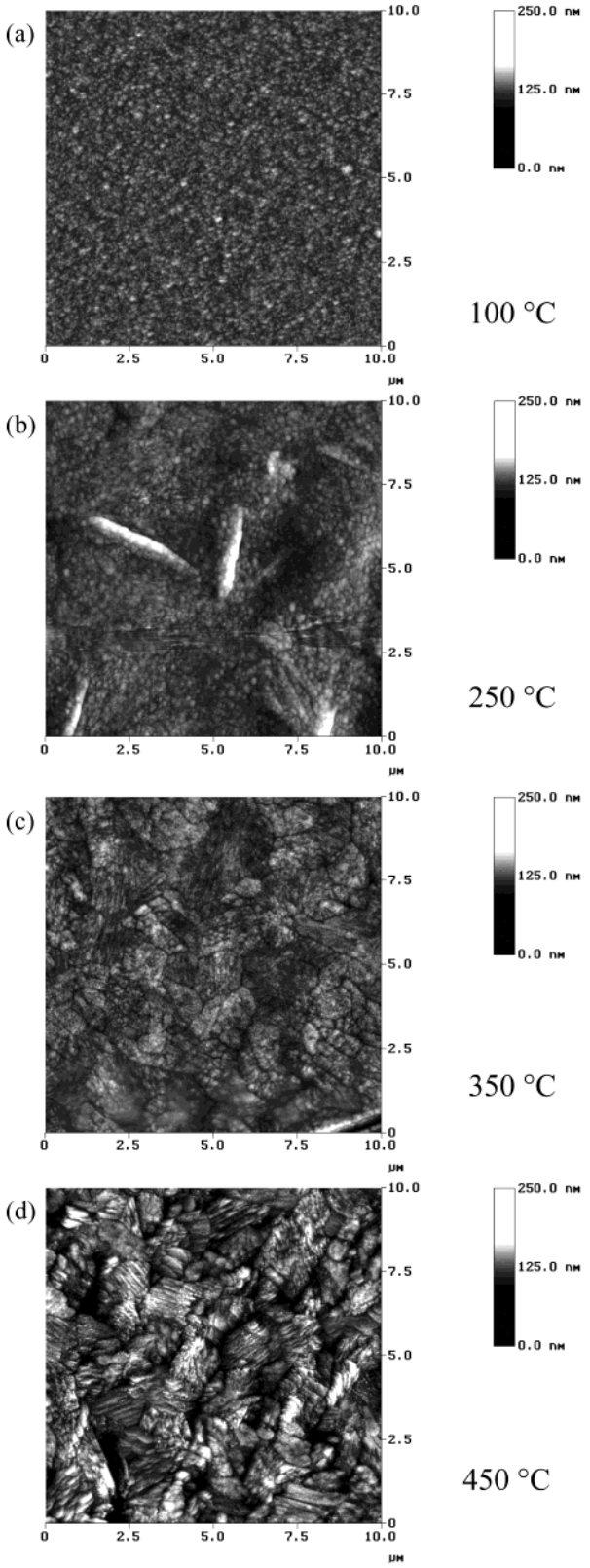

Figure 2. Representative AFM images ($10 \times 10\ \mu m^2$) of MoO_3 films sintered at (a) 100, (b) 250, (c) 350, and (d) 450 °C.

shift to higher binding energies is observed with the peak positions now located at 236.3 eV ($3d_{3/2}$) and 233.1 eV ($3d_{5/2}$). A slight shift of the same magnitude to higher energies was also found in the XPS core spectra of the O 1s electron as shown in Figure 4b. The ratio between the $3d_{5/2}$ and $3d_{3/2}$ peak areas after sintering is 4:3, indicating there is a conversion of the mixed-valent $Mo^{VI/V}O_{3-x}$ film

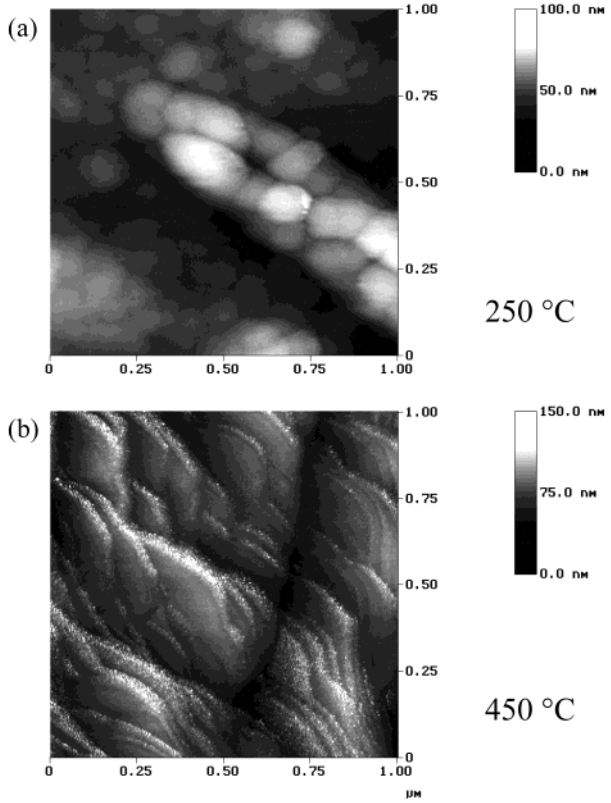

Figure 3. High-resolution AFM images ($1 \times 1\ \mu m^2$) of MoO_3 films sintered at (a) 250 and (b) 450 °C showing presence of microcrystallites and crystalline planes, respectively.

to more stoichiometrically pure $Mo^{VI}O_3$ film. A narrowing of both Mo 3d peaks as well as the O 1s peak is observed indicating an increase in overall film crystallinity.[16]

X-ray diffraction patterns showing the evolution from amorphous to crystalline MoO_3 thin films are shown in Figure 5. Sintering in air for 3 h at 25 and 100 °C produces films that are amorphous to X-rays with the only noticeable diffraction peaks being the reflections from the ITO substrate. Upon heating to 250 °C, peaks emerge which are attributed to the (020) and (040) reflections of a layered, orthorhombic α-MoO_3 with a third peak that can be assigned to reflections from either the (011) plane of α-MoO_3 or the (110) plane of the monoclinic, metastable β-MoO_3. The presence of the β-phase of molybdenum oxide at this temperature is supported by Kuzmin[30] and Julien[34] who have shown that sintering in air of hydrated, amorphous molybdenum oxide at relatively low temperatures produces a morphological change from an amorphous phase to a metastable, monoclinic β-MoO_3. Strict identification of β-MoO_3 is not possible, most likely because the average β-MoO_3 domain size is much less than cross sectional area of the X-ray probe beam or the β-MoO_3 exists as a nanocrystalline phase[35] and is too small to diffract the incident X-rays. To our knowledge this is the first report of the identification of β-MoO_3 in heat-treated thin

(34) Nazri, G. A., Julien, C. *Solid State Ionics* **1995**, *80*, 271.

(35) Preliminary Raman microprobe spectroscopy experiments indicate that several phases of MoO_3 are present. Some regions exhibit characteristic Raman shifts of 997, 821, and 668 cm^{-1} that are unique to α-MoO_3 while other regions exhibit Raman stretches at 850 and 776 cm^{-1} that are specific to β-MoO_3. These spectral assignments are in agreement to studies found in ref 37 and by Yebka, B.; Julien, C.; Nazri, G. A. *Mater. Res. Soc. Symp. Proc.* **1991**, *548*, 229. The lack of strong XRD peaks for β-MoO_3 and the presence of sharp Raman spectra is suggestive of nanocrystalline phases since the crystallite sizes are too small to diffract X-rays, yet are large enough to produce well-resolved Raman shifts.

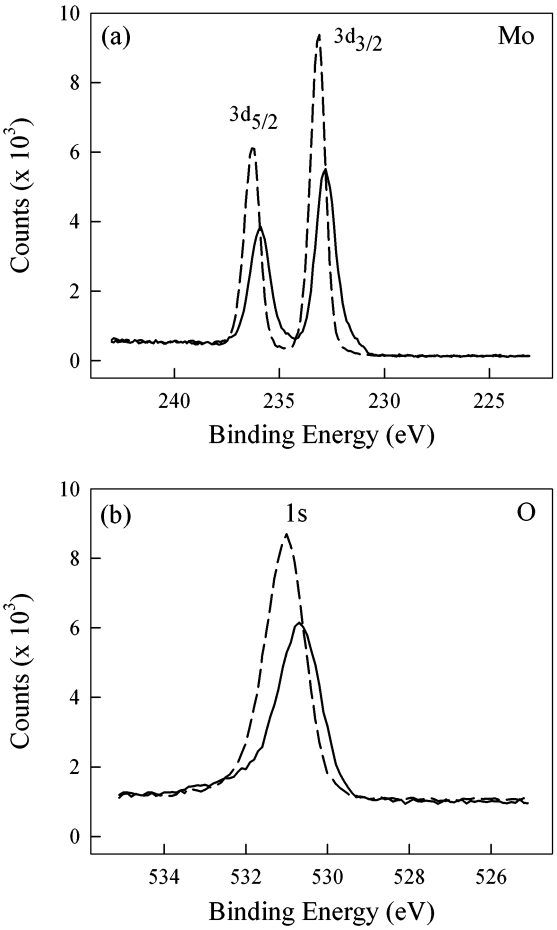

Figure 4. X-ray photoelectron spectra for a MoO_3 film (a) as deposited (solid line) and (b) sintered at 250 °C (dashed line). Results are shown for (a) Mo $3d_{3/2}$ and $3d_{5/2}$ and (b) O 1s.

films prepared by electrochemical deposition. To date, all other film preparation methods that are known to produce films comprising β-MoO_3 utilize spray pyrolysis or chemical vapor deposition techniques. Fabrication of films containing β-MoO_3 is quite interesting in that this phase has been found to be more catalytically active toward methanol oxidation than α-MoO_3.[36] Sintering for shorter times (i.e., 1 h) does not provide enough thermal energy to facilitate the conversion of the hydrated amorphous material to the more thermodynamically stable dehydrated α-MoO_3 phase or to the metastable β-MoO_3 phase. Sintering for longer times (>3 h) at elevated temperatures (>250 °C) produces crystalline films purely comprising α-MoO_3. Further heat treatment to 350 °C produces more crystalline films with sharper (020) and (040) peaks. Additionally, a new diffraction peak from the (021) plane of the α-phase appears, as well as, other higher index reflections [(101), (111), and (060)]. Heating to 450 °C produces no further significant changes to the diffraction pattern, which suggests that the film has been fully converted to α-MoO_3 by sintering at 350 °C for 3 h. Preferential growth along one axis during sintering is not observed, as evidenced by the presence of nearly equal intensities for all index reflections (i.e., *h*00 vs 0*k*0 reflections). X-ray diffraction measurements presented here, in addition to the morphological changes observed using AFM are consistent with previously published reports,[37] which indicate that extended sintering at 250

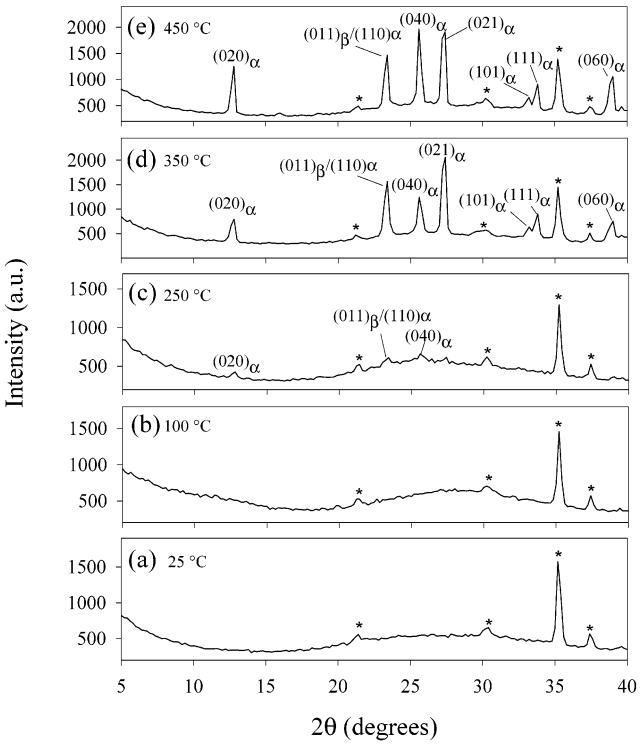

Figure 5. X-ray diffraction of a MoO_3 thin film (a) as deposited and subsequently sintered for 1 h at (b) 100, (c) 250, (d) 350, and (e) 450 °C. Asterisk denotes ITO peaks.

°C and above can induce a phase transition from an amorphous structure to a more thermodynamically stable, layered orthorhombic structure through water loss and film densification. As discussed in the following section, these structural changes significantly alter the ion insertion/expulsion kinetics due to changes in film structure, porosity, and active surface area.

Electrochemical Characterization. Qualitative analysis of the effects of sintering on the electroinsertion properties of MoO_3 thin films was carried out by performing cyclic voltammetry in propylene carbonate solutions containing 1 M $LiClO_4$. We have shown earlier that film deposition at −0.02 V vs Ag/AgCl produces a hydrated suboxide of molybdenum where the composition can be written as $MoO_{2.7}\cdot 2H_2O$.[22] As illustrated by the XPS and X-ray diffraction (XRD) data, postdeposition sintering of these films in air at elevated temperatures between 350 and 450 °C produces dehydrated, crystalline films comprising predominantly stoichiometric α-MoO_3. However, sintering at intermediate temperatures around 250 °C produces disordered mixed-phase films that are composed of a combination of amorphous MoO_3, nanocrystalline β-MoO_3, and partially crystalline α-MoO_3. The partially crystalline phase of α-MoO_3 present in films sintered at 250 °C, and above, is reported to consist of edge-sharing MoO_3 octahedra that form a layered structure with a spacing of about 6.9 Å between layers.[20] Presumably lithium transport is influenced by the formation of channels between these layers, which may provide facile ionic conduction pathways within the oxide film. These channels do not exist in films sintered at lower temperatures (25 and 100 °C). Figure 6 displays cyclic voltammograms acquired for films sintered in air for 3 h at (a) 100, (b) 250, (c) 350, and (d) 450 °C. Upon heating to 100 °C (Figure 6a), the observed voltammetric response

(36) Farneth, W. E.; McCarron, E. M., III; Sleight, A. W.; Staley, R. H. *Langmuir* **1987**, *3*, 217.

(37) Carcia, P. F.; McCarron, E. M., III *Thin Solid Films* **1987**, *155*, 53.

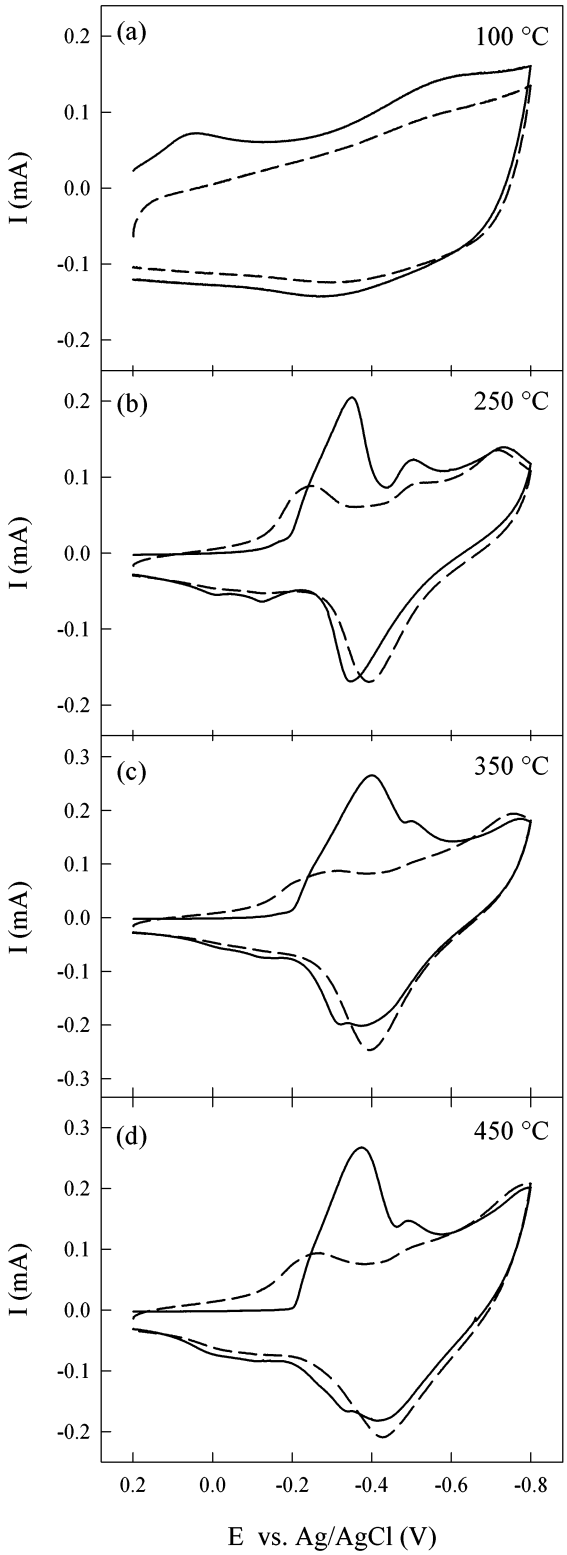

Figure 6. Voltammetric response (solid trace, first scan; dashed trace, second scan) of MoO_3 thin film electrodes immersed 1 M $LiClO_4$/PC as a function of sintering temperature. Traces plotted are for MoO_3 sintered for 3 h at (a) 100, (b) 250, (c) 350, and (d) 450 °C. Scan rate was 10 mV/s.

exhibits two very broad, ill-defined peaks, one centered at ~+0.04 V and the other at −0.6 V. The voltammetric response is rather capacitive and exhibits no defined reduction or oxidation peaks due to the bulk disorder in the film. On cycling a second time, the small peaks observed during the first insertion cycle disappear and the voltammetric response becomes even less resolved. A slight decrease in insertion capacity is also observed, but subsequent cycles are relatively constant after the second voltammetric cycle.

In contrast, the electrochemical responses for films sintered at higher temperatures (≥250 °C) are quite different (Figure 6b−d). The current responses for these films measured during the first voltammetric cycle (solid curves) exhibit at least three sets of distinguishable reduction and oxidation peaks. The presence of multiple peaks, as shown in Figure 6b, suggests the possibility that Li^+ insertion is occurring at energetically distinct reaction sites within the molybdenum oxide film. Further examination of voltammetric data shows that the first peak, centered at ca. −0.4 V is large on the first scan and decreases considerably on the second scan by nearly 75%. This type of response is most likely due to a combination of two factors: (1) faradaic electron transfer from the substrate to the MoO_3 film with concomitant Li^+ ion insertion and (2) a large capacitive charge arising from an electrochemically induced structural phase transition during Li^+ insertion.[38,39] Others have reported using XRD that the lattice spacing increases between 6.9 and 12.0 Å during the insertion process depending on the degree of Li^+ and solvent co-insertion.[25] Obviously, this electrochemically induced phase transition produces a significant alteration of the film structure. Integration of the cathodic and anodic peaks in Figure 6b after the first cycle indicates that the anodic peak area, associated with Li^+ deinsertion, is ca. 40% smaller, suggesting that the insertion/deinsertion process is only 60% reversible. This discrepancy cannot be due solely to slow diffusion of Li^+ during deinsertion; rather it is more likely due to some fraction of Li^+ becoming trapped in the film due to irreversible formation of a molybdenum bronze (i.e., $Li_{x+2}Mo^{VI}_{1-x}Mo^{V}_{x-z}Mo^{IV}_{z}O_{3-y-z}$) and/or due to solvent reduction/decomposition processes. This irreversible insertion is observed to an even greater extent with the insertion of larger cations such as Na^+ and Mg^{2+}.[40] Further, the inability to remove all the Li^+ stored in the film remains even if the potential is held at oxidizing potentials (i.e., +0.4 V vs Ag/AgCl) for extended lengths of time. Continued cycling of the potential (Figure 6b−d, dashed curves, second scan) shows the first reduction peak originally located at −0.4 V shifts to more a positive reduction potential and exhibits a large decrease in peak height as well as peak broadening. This suggests that Li^+ insertion is energetically more facile for MoO_3 films that possess some degree of inherent structural disorder. Dunn and co-workers[41] have reported similar findings for molybdenum oxide aerogels consisting of both amorphous and crystalline phases. Similar to our findings, a large activation peak appears on the initial insertion scan, which they have attributed to large structural changes in the aerogel upon Li^+ insertion. Consistent with Dunn et al., we also observe that the overall Li^+ insertion capacity slightly decreases (ca. 10%) upon repeated cycling (three to five cycles). This is also in agreement with other reports that have attributed this behavior to Li^+ accumulation at the MoO_3/ITO interface[5] and/or to film degradation processes.[42] We believe the observed loss in capacity is

(38) Conway, B. E. *Electrochemical Supercapacitors;* Kluwer Academic/Plenum Publishers: New York, 1999; p 248.
(39) Conway, B, E. *Electrochim. Acta* **1993**, *38*, 1249.
(40) Spahr, M. E.; Novak, P.; Haas, O.; Nesper, R. *J. Power Sources* **1995**, *54*, 346.
(41) Dong, W.; Mansour, A. N.; Dunn, B. *Solid State Ionics* **2001**, *144*, 31.
(42) Yoshiike, N.; Mizuno, Y.; Kondo, S. *J. Electrochem. Soc.; Solid-State Sci. Tech.* **1984**, *131*, 2634.

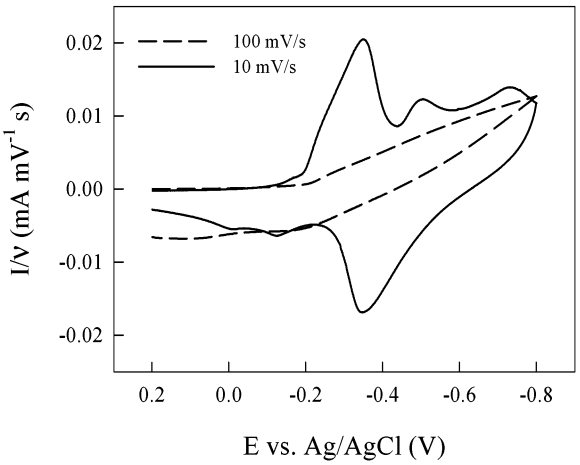

Figure 7. Voltammetric response for MoO_3 thin film electrodes immersed in 1 M $LiClO_4$/PC obtained using sweep rates of 10 mV/s (solid trace) and 100 mV/s (dashed trace).

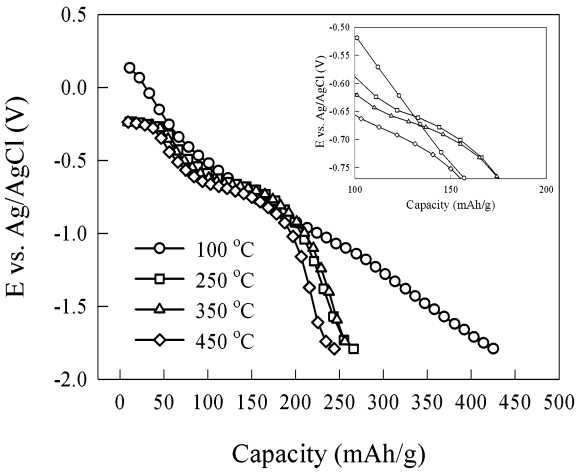

Figure 8. Discharge curves obtained in 1 M $LiClO_4$/PC solution, using MoO_3 thin film electrodes sintered at 100, 250, 350, and 450 °C. Inset: Magnification showing discharge capacity for intermediate values (0.5−1.3) of the mole fraction of Li^+ (in Li_xMoO_{3-x}). The applied current density was 10 μA/cm^2.

predominantly due to electrochemically induced structural changes during the initial reduction cycle. Consequently, mechanical material failure accompanying this electrochemically stimulated phase change results in active electrode area loss upon extended cycling. Parts c and d of Figure 6 show representative voltammetric responses for films annealed at (c) 350 °C and (d) 450 °C. The voltammetric response is comparable to those films sintered at 250 °C; however, these films are rather unstable toward extended insertion/deinsertion cycling, as indicated by large portions of the films delaminating from the substrate, thus permanently deactivating these portions for further electroinsertion activity.

In contrast to our cyclic voltammetry results and those of Dunn and co-workers,[41] Dao and co-workers have reported that Li^+ insertion/deinsertion into electrochemically deposited MoO_3 is characterized by a voltammetric response void of any well-defined reduction peaks.[15,16] However, in their experiments the potential was only scanned as far negative as −0.5 V vs Ag/AgCl, a potential range that coincides with the peak potential involving only the first reduction peak. In addition, measurements made by Maruyama and Kanagawa[43] on crystalline MoO_3 prepared by chemical vapor deposition using a potential sweep rate of 100 mV/s showed that there was an absence of defined reduction peaks during electrochemical Li^+ insertion even when the potential was scanned as far negative as −1.0 V vs SCE. Most likely their observed voltammetric responses are dominated solely by resistive charging processes ("IR-drop") due to sluggish ion transport as the scan rate exceeds the diffusive component to solid-state diffusion of Li^+ within the MoO_3 film. We observe a definitive scan rate dependence on the voltammetric response recorded during potential sweep experiments. For example, Figure 7 demonstrates the influence of scan rate on the measured voltammetric response. If a scan rate of 10 mV/s is used (solid curve), multiple reduction and oxidation peaks are observed for MoO_3 thin film electrodes sintered at 250 °C on both reduction and oxidation cycles. However, if the scan rate is increased to 100 mV/s (dashed curve), the observed voltammetric response for a film prepared in the same manner exhibits only a large, sloping cathodic current beginning at −0.2 V that continues to −0.8 V. Additionally, two small anodic peaks located at −0.2 and +0.1 V are observed during the return wave. The faster scan rate response is similar to that reported by Dao[15,16] and by Maruyama and Kanagawa[43] where their results showed a single ill-defined cathodic peak and two barely discernible anodic peaks. "Fast" scan rate studies ($\nu \geq 100$ mV/s) are suitable for investigations involving solution phase redox chemistry, where ionic diffusion is on the order of 10^{-5} cm^2/s, but not for electroinsertion experiments where solid-state diffusion is expected to be about 3−8 orders of magnitude slower.

Galvanic discharge curves were also performed to determine the insertion capacity for Li^+ in films sintered at each of these different temperatures. Figure 8 shows typical discharge curves obtained from MoO_3 films sintered in air for 3 h at 100, 250, 350, and 450 °C. The film sintered at 100 °C exhibited nearly monotonic, sloping cell voltage decays, whereas more dehydrated films (≥250 °C) exhibited voltage decays possessing both sloping and flat regions. In general, discharge curves possessing features characterized by sloping decay responses are indicative of insertion into a host material comprising a single phase; whereas discharge curves possessing flat regions of near constant cell voltage (i.e., plateaus) imply that the host material is composed of at least two chemically distinct phases. Two plateaus are evident in the discharge curves for films sintered at higher temperatures (≥250 °C) within the capacity ranges of 0−50 mA h/g and 100−150 mA h/g. A very sharp initial decrease in cell voltage is also observed for the higher temperature sintered films upon commencement of the galvanostatic experiment, which is consistent with our voltammetric results presented above, and suggestive of the influence of electrochemically induced structural changes. As reported by Julien and co-workers,[44−46] when discharge curves are performed on hydrated molybdenum oxides from open circuit potential down to −0.77 V vs Ag/AgCl (2.5 V vs Li/Li^+), dehydrated films show a higher insertion capacity than hydrated oxide films. This general trend is observed in the data shown in Figure 8 for films discharged down to −0.77 V (see inset). Films sintered at 100 °C exhibit a lower ion storage capacity (154 mAh/g) compared to films prepared at higher temperatures (250 °C, 173 mA

(43) Maruyama, T.; Kanagawa, T. *J. Electrochem. Soc.* **1995**, *142*, 1644.

(44) Nazri, G. A.; Julien, C. *Ionics* **1996**, *2*, 196.

(45) Guzman, G.; Yebka, B.; Livage, J.; Julien, C. *Solid State Ionics* **1996**, *86−88*, 407.

(46) Yebka, B.; Julien, C.; Nazri, G. A. *Ionics* **1999**, *5*, 236.

h/g; 350 °C, 175 mA h/g; 450 °C, 155 mA h/g). These capacity values correspond to Li:Mo mole fractions (x in $Li_xMo^{VI}_{1-x}Mo^{V}_{x}O_{3-x}$) of 0.93, 0.94, 0.95, and 0.85 for films sintered at 100, 250, 350, and 450 °C, respectively. In contrast, the insertion capacity trend is reversed when the films are subjected to deep discharge conditions (ca. −1.8 V vs Ag/AgCl or ∼1.5 V vs Li/Li^+). Under these conditions, the films that are more amorphous and presumably contain more water and oxygen deficiencies (i.e., sintered at 100 °C) exhibit a much larger insertion capacity than those films that are more crystalline and dehydrated. The experimentally determined capacities and corresponding Li^+:Mo mole fractions for films sintered at 100, 250, 350, and 450 °C were found to be 426 (2.6 Li:Mo), 268 (1.5 Li:Mo), 264 (1.4 Li:Mo), and 244 mAh/g (1.3 Li:Mo), respectively, under deep discharge conditions. Similar lithium insertion capacities have been reported by Dunn et al.,[41] for aerogels of amorphous and crystalline MoO_3, although we found a much higher capacity for amorphous films of MoO_3. We observe that for all of these films studied, independent of the sintering temperature, the charge capacity (deinsertion) was ∼50% less than the discharge capacity (insertion), suggesting that irreversible film reduction occurred during deep discharge conditions. This irreversible insertion behavior is most likely a result of potential-induced structural deformation processes and to the formation of electrochemically inactive reduction products (e.g., reduced lithium bronze phase). Both of these effects contribute to redox deactivation and mechanical failure of MoO_3, thus preventing the reversible reoxidation of some portions of the cathode material. It is also likely that deep discharge conditions lead to the formation of solid electrolyte interphase (SEI) layers that consist of electrolyte decomposition products (e.g., polymeric compounds, lithium alkyl carbonates, and lithium oxide).[47] SEI layers in effect act to passivate and deactivate portions of the MoO_3 film.

Spectroelectrochemical Characterization. Figure 9 shows absorption spectra of sintered MoO_3 films that were acquired during a voltammetric sweep from +0.4 to −0.8 V. In Figure 9a, potential-dependent absorption spectra are displayed for a MoO_3 film sintered at 100 °C. For clarity, only 5 of the 120 spectra collected during the experiment are shown. At the start of the experiment, the film has a slight blue color indicated by a broad near-IR absorption in the UV−vis spectrum. As the potential is scanned to negative values, an increase in near-IR absorbance is seen, as expected, due to the reduction of MoO_3 and formation of a $Li_xMo^{VI}_{1-x}Mo^{V}_{x}O_{3-x}$ bronze. After the switching potential at −0.8 V is reached, the absorbance in the near-IR begins to decrease. The absorbance spectrum of the reoxidized film closely resembles that of the film in its original oxidized state. A more illustrative example of the reversibility of the potential-dependent absorbance is shown in Figure 9b. Both the voltammetric response (Figure 6a) and the optical absorbance steadily increase immediately after commencement of the potential scan. This indicates that low overpotentials can be used to effectively reduce Mo^{VI} to Mo^{V} when the MoO_3 film is structurally amorphous, hydrated, and chemically mixed-valent. When the applied potential reaches ca. −0.4 V, the absorbance becomes constant, most likely due to a filling of available insertion sites within the film. A slight decrease in absorbance is observed as the potential reaches −0.8 V. This decrease could be due either to film dissolution or to the formation of a lower suboxide of molybdenum

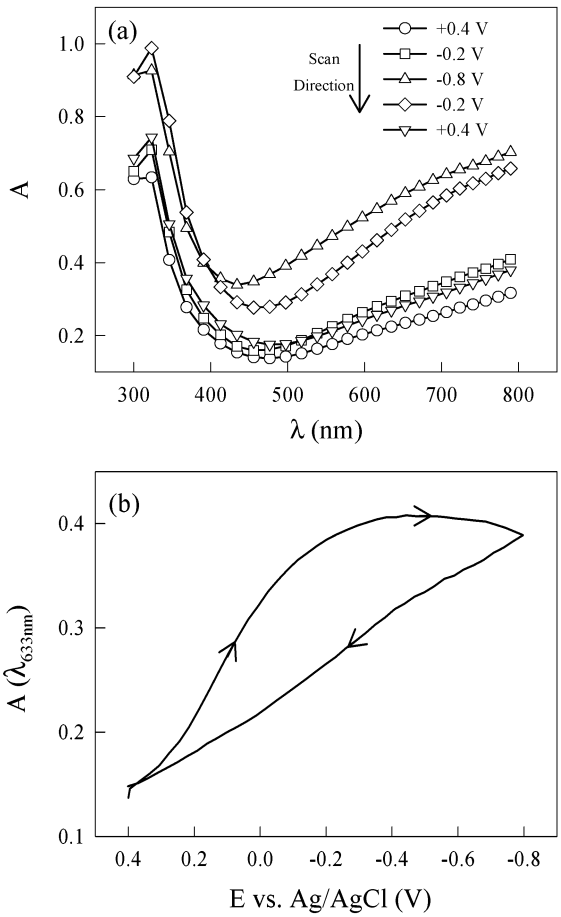

Figure 9. Spectroelectrochemical response in 1 M $LiClO_4$/PC solution of a MoO_3 thin film electrode sintered at 100 °C for 3 h: (a) optical absorption spectra obtained during a potential sweep; (b) plot of absorbance at 633 nm vs potential for the spectroelectrochemical experiment in (a).

(i.e., $Li_{x+2}Mo^{VI}_{1-x}Mo^{V}_{x-z}Mo^{IV}_{z}O_{3-y-z}$) resulting in a change in the molar absorptivity of the film. The coloration efficiency ($\Delta OD/Q$) for the forward coloration sweep was calculated to be 6.3 cm^2/C. Scanning back to +0.4 V causes reoxidation of the film (Li^+ expulsion), and a nearly linear decrease in absorbance is observed. Presumably, reoxidation of the film causes lithium to deinsert at potentials more negative than where it originally inserted because lithium is being extracted from two chemically distinct molybdenum oxides, each of which exhibits markedly different oxidation potentials. It should also be noted that the coloration process is almost completely reversible with an overall coloration reversibility estimated to be ∼93.4%.

In comparison, Figure 10 shows the results from a spectroelectrochemical experiment using MoO_3 thin films sintered at 250 °C. Figure 10a shows spectra acquired during a voltammetric sweep from +0.4 to −0.8 V. Initially, the film at +0.4 V is slightly yellow in color as indicated by the small absorption band at 450 nm. When the potential is scanned more negative, a slight increase in near-IR absorbance is observed near −0.2 V, whereupon further scanning to more negative potentials causes the film to develop a deep blue color, which is attributed to the formation of a mixed-valent $Li_xMo^{VI}_{1-x}Mo^{V}_{x}O_{3-x}$ bronze. Reversal of the voltammetric sweep direction results in film decoloration as evidenced by the observed decrease in absorbance. When the potential reaches +0.4 V, the resulting absorption spectrum is quite different compared to the spectrum prior to insertion, as signified by the retention of a significant near-IR absorbance even

(47) Peled, E.; Bar Tow, D.; Merson, A.; Gladkich, A.; Burstein, L.; Golodnitsky, D. *J. Power Sources* **2001**, *97−98*, 52.

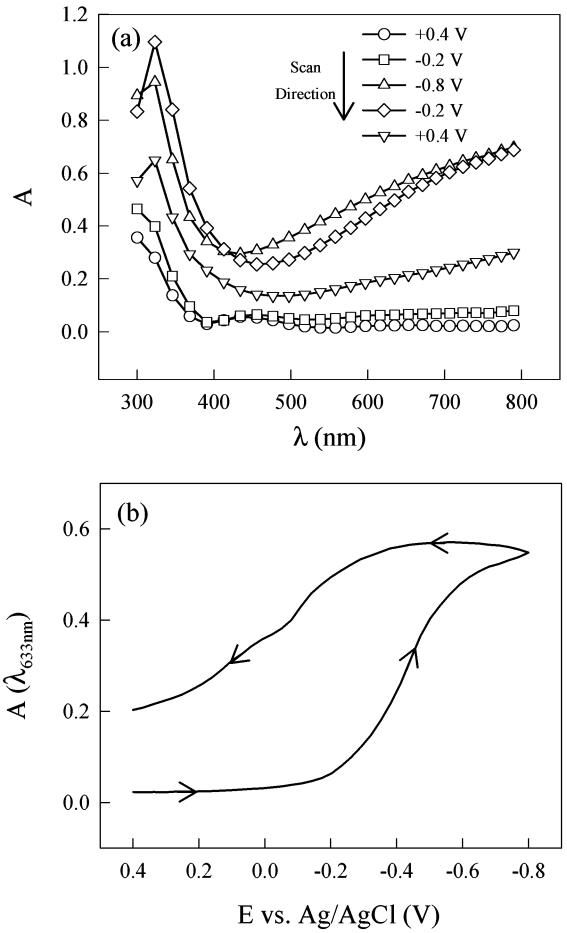

Figure 10. Spectroelectrochemical response in 1 M $LiClO_4$/PC solution of a MoO_3 thin film electrode sintered at 250 °C for 3 h: (a) optical absorption spectra obtained during a potential sweep; (b) plot of absorbance at 633 nm vs potential for the spectroelectrochemical experiment in (a).

at very oxidizing potentials. Figure 10b illustrates the coloration behavior in a different fashion, where the potential-dependent absorbance at 633 nm is plotted as a function of the applied potential. The shape of the absorbance vs potential plot during reduction resembles that of the current response (see Figure 6b) where negligible change in absorbance, or current, is observed until the potential reaches ca. −0.2 V. When this potential is reached, steep increases in both absorbance and current are observed with the absorbance growing until the potential reaches −0.6 V, after which it begins to level off. As the potential is scanned positive toward more oxidizing potentials, the absorbance remains nearly constant until about −0.3 V, after which there is a slow decrease. This behavior suggests that the decoloration (deinsertion) process is kinetically slower and thermodynamically hindered, in contrast to decoloration (deinsertion) of an amorphous MoO_3 thin film (refer to Figure 9). Comparison of the curves in Figures 9b and 10b shows that MoO_3 films sintered at 250 °C exhibit a larger optical modulation albeit with the sacrifice of optical and electrochemical reversibility. The coloration efficiency calculated for films sintered at this temperature is ∼15.8 cm^2/C—twice as large as that measured for amorphous films. However, the resulting electrochromic reversibility was also significantly less than that of the amorphous MoO_3 thin film (cf. 67.2% vs 93.4%).

A more quantitative electrochemical approach to study the effects of sintering conditions on the electroinsertion

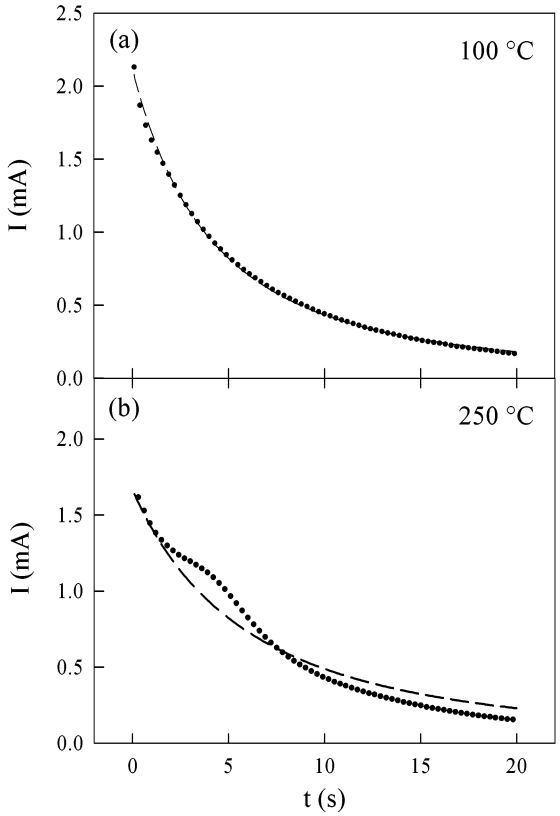

Figure 11. Current response recorded during a potential step from +0.4 to −0.8 V for MoO_3 thin film electrodes sintered at (a) 100 and (b) 250 °C immersed 1 M $LiClO_4$/PC. Solid circles and dashed curve represent experimental data and experimental fits, respectively.

properties involved the use of chronoamperometry. Under conditions of solid-state semi-infinite linear diffusion,[48] analysis of current transients measured during a potential step[49] to reducing potentials allows for the determination of apparent Li^+ diffusion coefficients (D_{Li^+}) within MoO_3 thin films. A representative set of chronoamperometry data for MoO_3 thin films sintered at 100 and 250 °C, each for 3 h, is shown in Figure 11. The chronoamperometric response (solid circles) for a MoO_3 thin film sintered at 100 °C during a potential step to −0.8 V (Li^+ insertion) is shown in Figure 11a. The data fit (dashed line) is excellent with an R^2 value >0.99. D_{Li^+} was calculated to be 4.9×10^{-12} cm^2/s, which is in good agreement with other values for reported amorphous MoO_3 films.[1] In contrast, the current response for a film sintered at 250 °C, shown in Figure 11b, does not exhibit classical Cottrell behavior ($t^{-1/2}$ current decay). Therefore, the fit (dashed line) is somewhat erroneous, considering the experimental transient response (solid circles) is actually composed of two components —a small region from 0 to ∼2 s and a larger region from ∼2 to 20 s. Although the fit is very poor, D_{Li^+} was estimated to be $\sim 2 \times 10^{-12}$ cm^2/s. While the estimated D_{Li^+} for polycrystalline MoO_3 agrees with reported values for lithium diffusion found using chronoamperometry,[1] quantitative interpretation of the data proves to be somewhat complicated due to the difficulty in interpreting the non-Cottrell type transient response. Cottrell conditions do not account for microscopic variations in surface topography nor do they include the possibility of varied ionic diffusion rates at an electrode

(48) Wen, C. J.; Boukamp, B. A.; Huggins, R. A.; Weppner, W. *J. Electrochem. Soc., Solid-State Sci. Technol.* **1979**, *126*, 2258
(49) Craig, J. B.; Grant, J. M. *J. Mater. Chem.* **1992**, *2*, 521.

surface composed of multiple phases with energetically distinct reaction sites. These two contributing factors must be considered in light of the AFM analysis presented in Figures 2 and 3, which show that a MoO_3 thin film sintered at 250 °C is actually composed of a mixture of amorphous, nanocrystalline, and randomly oriented crystalline domains. MoO_3 has been known to exist in several phases, each with different electronic conductivities, which have been reported to differ over 7 orders of magnitude.[50] Over the studied temperature range of 25−250 °C, the three most dominant phases of MoO_3 are a hydrated amorphous phase, a metastable, rhenium oxide-like phase denoted as β-MoO_3, and a layered, thermodynamically stable phase, indicated as α-MoO_3. The observed anomalous electrochemical behavior in the MoO_3 thin films (250 °C) is due, in part, to a coupling of the chemical reactivity of different phases of molybdenum oxide (i.e., β- and α-MoO_3) giving rise to multiple peaks in the cyclic voltammogram. The key aspect is that the ensemble response is not simply equal to the average of the responses from all individual domains. Instead, isolated domains of the mixed-phase material exhibit unique and diversely different time-dependent behaviors.

Some authors have reported that chemical diffusion coefficients for species in the solution phase[51] and in the solid state[52,53] can be determined using chronoamperometry coupled with optical absorption measurements. The major drawback to spectroelectrochemical characterization using potential sweep (cyclic voltammetry) or potential step (CA, CC) experiments coupled to conventional UV−vis spectroscopy is that both measurements (optical and electrochemical) are based on the measurement of an ensemble response. If films are heterogeneous structurally and/or chemically on a microscopic size scale, difficulty arises in the ability to resolve contributions from individual domains to the overall electrochemical/electrochromic response. The structural inhomogeneities are suggestive of spatially localized electrochemical activity, evidenced by the existence of complicated voltammetric and electrochromic responses that display features characteristic of energetically distinct phases and domain-specific reactivity. In an attempt to confirm this hypothesis, we have conducted preliminary studies of these mixed phase films using a newly developed spectroelectrochemical imaging technique. Such an experiment is shown in Figure 12, where transmitted light images were collected as a function of potential at oxidized (deinserted state) and subsequent reducing potentials (insertion). In Figure 12a, an optical micrograph (75 × 75 μm^2 area) of an oxidized MoO_3 film prior to Li^+ insertion is shown. The film consists of numerous grains of varying size, orientation, and degree of crystallinity, supporting our assessment that these films are indeed polycrystalline. Figure 12b shows an optical micrograph of the same film (and area) shown in Figure 12a undergoing Li^+ insertion as the potential is stepped to −0.8 V vs Ag/AgCl. As seen in Figure 12b, upon reduction, Li^+ enters the film, resulting in a high degree of structural distortion and nonuniform coloration. The various gray scale intensities observed in distinct regions are indicative of different degrees of coloration and consequently suggest differing degrees of Li^+ insertion reactivity. Normally, when the equivalent spectroelectrochemical experiment is conducted using a conventional UV−vis spectrometer, it is assumed that the material responds optically and electrochemically in a homogeneous manner. Clearly, this is not the case for thin films prepared at this sintering temperature. This may help explain the large variation in reported behaviors for MoO_3 prepared by various methods and procedures. These films not only are heterogeneous structurally but also exhibit inhomogeneous ion/charge-transfer reactivity toward lithium insertion. Through spatially resolved elucidation of electrochemical reactivity at individual domains of different crystallinity and chemical composition, we hope to gain a more fundamental understanding of the relationships between surface morphology, chemical composition, and ion/charge-transfer reactivity. A more detailed description of this experimental approach and results obtained using this new methodology in the study of electroinsertion/electrocoloration in thin films of MoO_3 will be reported in a forthcoming publication.[54]

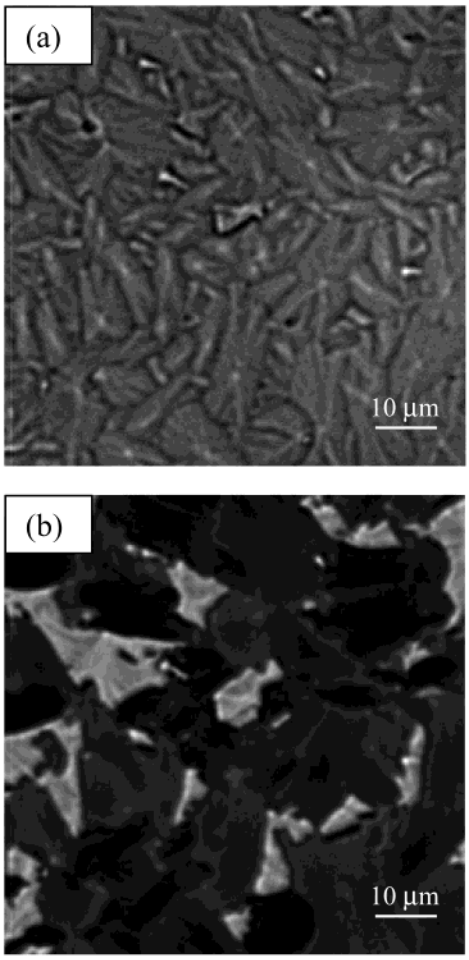

Figure 12. Optical micrographs (75 × 75 μm^2) of Li^+ insertion in a MoO_3 thin film sintered at 250 °C: (a) initial image of a MoO_3 film poised at +0.4 V (vs Ag/AgCl) prior to insertion of Li^+; (b) image of the same area poised at −0.8 V during lithium insertion.

4. Conclusions

In this work we have shown that sintering of MoO_3 thin films in air at different temperatures directly influences the observed electrochromic and electroinsertion characteristics through modification of film micro/nanostructure. Films sintered at relatively low temperatures (100 °C) are mixed valent ($Mo^{VI/V}$), amorphous, contain a

(50) Robin, M. B.; Day, P. In *Advances in Inorganic Chemistry and Radiochemistry;* Emeleus, H. J., Sharpe, A. J., Eds.; Academic Press: New York, 1967; p 335.
(51) Li, C-yu; Wilson, G. S. *Anal. Chem.* **1973**, *45*, 2370.
(52) Cheng, G.; Dong, S. *Electrochim. Acta* **1987**, *32*, 1561.
(53) Vuillemin, B.; Bohnke, O. *Solid State Ionics* **1994**, *68*, 257.
(54) McEvoy, T. M.; Stevenson, K. J. In preparation.

significant amount of water, and exhibit facile optical and electrochemical reversibility. On the other hand, more dehydrated, stoichiometrically pure $Mo^{VI}O_3$ can be prepared by sintering at temperatures greater than 250 °C. We also found that sintering of MoO_3 thin films at 250 °C produces a mixed-phase material that provides a larger optical modulation than for MoO_3 thin films sintered at 100 °C, with the sacrifice of electroinsertion reversibility.

Acknowledgment. K.J.S., J.T.H., and X.D. thank Dr. Suzanne Bélanger for assistance with the XRD measurements and gratefully acknowledge the Office of Naval Research for financial support. T.M.M. and K.J.S. thank the Welch Foundation and the National Science Foundation for funding as well.

LA027020U